Vibrational Analysis of $I_2^{\bullet-}.nCO_2$ Clusters ($n = 1-10$): A First Principle Study on Microsolvation

A. K. Pathak,[†] T. Mukherjee,[†] and D. K. Maity*[,‡]

Radiation and Photochemistry Division, and Theoretical Chemistry Section, Chemistry Group, Bhabha Atomic Research Centre, Mumbai 400085, India

Received: June 18, 2008; Revised Manuscript Received: September 20, 2008

Structure, stability, and vibrational IR and Raman spectra of $I_2^{\bullet-}.nCO_2$ clusters ($n = 1-10$) are reported based on first-principle electronic structure calculations. Several close-lying minimum energy structures are predicted for these solvated clusters following the quasi Newton−Raphson procedure of geometry optimization. Search strategy based on Monte−Carlo simulated annealing is also applied to find out the global minimum energy structures of these clusters. Successive addition of solvent CO_2 molecules to the negatively charged diatomic solute, $I_2^{\bullet-}$, is fairly symmetrical. Energy parameters of these solvated clusters are calculated following second-order Moller−Plesset perturbation (MP2) as well as coupled cluster theory with 6−311+G(d) set of basis function (I atom is treated with 6−311G(d) set of basis function). The excess electron in these solvated clusters is observed to be localized mainly over the two I atoms. Average interaction energy between the anionic solute, $I_2^{\bullet-}$, and a solvent CO_2 molecule is ∼129 meV in $I_2^{\bullet-}.nCO_2$ clusters, and the average interaction energy between two solvent CO_2 molecules is ∼85 meV in the case of neutral $(CO_2)_n$ clusters at MP2 level of theory. IR spectra show similar features in all these solvated clusters, depicting a strong band at ∼2330 cm^{-1} for C−O stretching and a weak band at ∼650 cm^{-1} for CO_2 bending modes. Degeneracy of the bending mode of a free solvent CO_2 unit gets lifted when it interacts with the charged solute $I_2^{\bullet-}$ to form a molecular cluster because of the change in structure of solvent CO_2 units. The vibrational band at the bending region of CO_2 in the Raman spectra of these anionic clusters shows a characteristic feature for the formation of $I_2^{\bullet-}.nCO_2$ clusters showing a Raman band at ∼650 cm^{-1}.

1. Introduction

Molecular clusters have been the subject of intense research in recent years because of the large dependency of cluster properties on size and shape. Molecular clusters of a solute wrapped in solvent molecules offer a unique opportunity to study the evolution of solvation motif and properties on successive addition of solvent molecules. Of late, size-selected cluster spectroscopy combined with first-principle-based theoretical calculation has become a powerful tool to obtain molecular level information on the solvation process of a solute. When a charged solute is added into a solvent continuum, the preexisting solvent interactions get modified to provide accommodation for the solute in the best possible way. Positively charged solute (cation) has a simple solvated structure and a solvation process easy to understand compared to a negatively charged solute (anion) as a cation binds strongly with solvent molecules.[1] The electron distribution pattern of a negatively charged solute plays the key role to shape up the structure of the solvent network surrounding the solute. A delicate balance between solvent−anion and solvent−solvent interactions determines the structure of a solvated anion cluster. In this regard, a substantial amount of research has been carried out on hydration of a negatively charged solute, and a large number of reports are available in the literature based on theoretical and experimental studies.[1−16]

As anions are mass selectable and have weak interaction with solvent molecules, the small anionic clusters having negatively charged chromophore have considered as model systems for studying the influence of solvation on various fundamental molecular properties and processes.[17,18] In this regard, iodine dimer radical anions ($I_2^{\bullet-}$) embedded in the Ar, CO_2, OCS solvents have been studied extensively by different research groups applying experimental and theoretical techniques.[19−30] Recently, a study based on first-principle electronic structure theory has been reported on iodine dimer radical anion ($I_2^{\bullet-}$) embedded in strongly interacting solvent water molecules.[31] A method of cluster calorimetry by femtosecond stimulated emission pumping has also been applied to measure the solvent stabilization energies of the first eight solvent CO_2 molecules in $I_2^{\bullet-}.nCO_2$ clusters.[32] Photoinduced dissociation and recombination dynamics of weakly interacting clusters of solute $I_2^{\bullet-}$ and solvent Ar, CO_2, and OCS molecules have been studied by femtosecond photoelectron spectroscopy and time-resolved absorption recovery experiments exploring fundamental questions about the dynamics of photochemical dissociation in clusters and in solutions. Evidence of spin orbit relaxation and photofragment caging due to asymmetric solvation have also been reported on these cluster systems. Theoretical treatments on these cluster systems have used either molecular dynamics simulation based on purely empirical force fields or semiempirical effective Hamiltonian models in which the electrons on the solute are treated quantum mechanically but the solvent molecules are treated classically. These treatments have been fairly successful to interpret the observed behavior of the caging in terms of the calculated equilibrium cluster structures. In particular, the onset of complete caging has been shown to correspond to the formation of a complete solvent shell around the solute. However, an accurate treatment of all electrons on

* E-mail for correspondence: dkmaity@barc.gov.in.
[†] Radiation and Photochemistry Division.
[‡] Theoretical Chemistry Section.

10.1021/jp805348q CCC: $40.75
Published on Web 11/06/2008

TABLE 1: Comparison of Experimental and Calculated Geometrical Parameters of the Mono Carbon Dioxide Cluster of $I_2^{\bullet-}$ ($I_2^{\bullet-}.CO_2$), Applying Different Popular Theoretical Methods That Adopt the 6-311+G(d) Set of Basis Functions (I is treated by 6-311G(d))

method	I···I Distance (Å)	I···C distance (Å)	O−C distance (Å)	∠OCO (deg)
MP2	3.281	3.728	1.170	176.5
BHHLYP	3.332	3.903	1.147	176.4
B3LYP	3.400	3.980	1.160	176.4
Expt[a]			1.162	177.5

[a] Reference 28

solute and solvent in such clusters is warranted to describe the process of microsolvation in the presence of weakly interacting solvents such as CO_2 especially in the connection of solute to solvent charge flow and asymmetric solvation. In the case of $I_2^{\bullet-}.nCO_2$ clusters, full ab initio treatment of all electrons on solute and solvent has been applied for $n = 1$ mainly to understand the structural aspects.[28] To the best of our knowledge, no attempt has been made to study structure and properties of higher solvated clusters of $I_2^{\bullet-}$, i.e., clusters with more than one solvent CO_2 molecule, applying the first-principle-based procedure. Vibrational Raman spectroscopy has been widely used to describe the interactions of solvent water molecules with a solute, aqueous interface, and nanodrops.[33] The strong Raman signal of the H−O−H bending mode of solvent H_2O molecule has been proposed to be used as a fingerprint to address the local microstructures of solvent water molecules in aqueous chemical and biological systems.[34] Thus, it will be interesting to perform such spectroscopic studies in the case of $I_2^{\bullet-}.nCO_2$ clusters, characterizing the specific interactions between solute $I_2^{\bullet-}$ and solvent CO_2 molecules as well as between two solvent CO_2 molecules. In what follows, we present a systematic first-principle-based theoretical study on structure, energy, and vibrational spectroscopic aspects of $I_2^{\bullet-}.nCO_2$ clusters ($n = 1-10$) to elucidate the effect of microsolvation of solute $I_2^{\bullet-}$ in solvent CO_2.

2. Theoretical Method

Full geometry optimizations are carried out adopting a hybrid density functional, namely, Becke's half-and-half (BHH) nonlocal exchange and Lee−Yang−Parr (LYP) nonlocal correlation functionals (BHHLYP) with triple split valence, 6−311+G(d) set of basis function (I is treated with 6−311G(d) basis set). It is reported in the literature that BHHLYP functional performs well to describe such open shell doublet systems.[35,36] Energy parameters are further improved by single point energy calculations applying second-order Moller−Plesset (MP2) perturbation theory adopting 6−311+G(d) basis sets. The quasi Newton−Raphson-based algorithm is applied to carry out geometry optimization for each of these molecular clusters with various initial structures designed systematically following a bottom-up approach to determine the most stable one. This procedure involves the calculation of a multidimensional potential energy surface for these molecular clusters and finding a minimum on the surface. The key issue in this search procedure is to estimate a good starting geometry of the cluster, which might converge during the calculation to a local or the global minimum. It is to be noted that the adopted procedure for geometry optimization cannot guarantee to locate the global minimum energy structure especially for the higher molecular clusters. Thus, Monte−Carlo-based simulated annealing procedures are also applied with the effective fragment solvent CO_2 molecules to find out the global minimum energy structure of different size molecular clusters.[37] In this method, molecular coordinates are displaced by a random amount and the energy of the system has been evaluated at the new structure. The new structure with lower energy is accepted while structures with higher energies have been accepted at a probability determined by the Boltzmann factor. Random structures are generated by carrying out Monte−Carlo steps at a high temperature (20 000 K) for more than 1000 steps. Hessian calculations are performed for all the optimized minimum energy structures to check the nature of the equilibrium geometry and to generate IR and Raman spectra. All these calculations are carried out applying the GAMESS program system on a LINUX cluster platform.[38] Visualization of molecular geometry, orbital, normal modes, and IR spectra is carried out by the MOLDEN program system.[39] Basis sets 6−311G(d) for I are obtained from the Extensible Computational Chemistry Environment Basis Set Database, Pacific Northwest National Laboratory.

3. Results and Discussion

The calculated bond distance of iodine dimer radical anion ($I_2^{\bullet-}$) is 3.334 and 3.285 Å at BHHLYP and MP2 levels of theory, respectively, adopting a triple split Gaussian valence 6−311G(d) basis set. However, the popular DFT functional, namely, B3LYP, yields a much longer I···I distance (3.402 Å) as reported by Neumark and co-workers.[28] The binding energy of $I_2^{\bullet-}$ is calculated as 1.19 and 1.12 eV, and the vertical detachment energy (VDE) for $I_2^{\bullet-}$ is predicted as 3.92 and 3.40 eV at the two theoretical levels, BHHLYP and MP2, applying the same set of basis functions. An accurate level of theory, namely, CCSD(T)/6−311G(d), estimates the binding energy and VDE of this doublet radical anion as 1.06 and 3.12 eV, indicating large overestimation of same by the present DFT method.

3.1. Structure. To select an appropriate theoretical method, geometrical parameters of $I_2^{\bullet-}.CO_2$ are calculated applying correlated hybrid density functionals (B3LYP and BHHLYP) as well as second-order Moller−Plesset perturbation theory adopting 6−311+G(d) basis function (6−311G(d) basis set for the I atom). It is observed that Becke's half-and-half (BHH) nonlocal exchange and the Lee−Yang−Parr (LYP) nonlocal correlation functional (BHHLYP) performs well to describe such molecular clusters producing geometrical parameters close to the MP2 method. The present calculated geometrical parameters of this cluster are compared in Table 1 along with earlier reported results for this monosolvated cluster. It is clearly observed that BHHLYP performs better than B3LYP functional with reference to MP2 results. It is also reported in the literature that BHHLYP functional performs well to describe such open shell doublet systems.[35,36] Thus, BHHLYP hybrid DFT functional is adopted for all $I_2^{\bullet-}.nCO_2$ clusters studied at present.

The most stable structure of monosolvated cluster $I_2^{\bullet-}.CO_2$ calculated at BHHLYP level of theory is shown in Figure 1A. It is interesting to note that the CO_2 moiety in the cluster is near perpendicular to the I···I axis in the most stable structure, an initial guess structure where the CO_2 moiety is

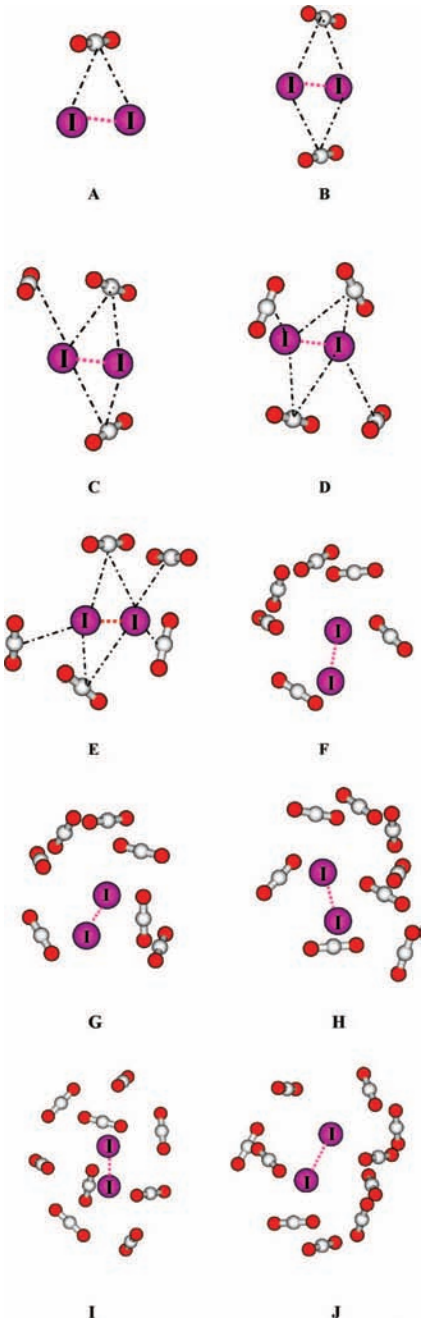

Figure 1. Optimized most stable structure calculated at BHHLYP/6−311+G(d) level of theory for (A) $I_2^{\bullet-}.CO_2$, (B) $I_2^{\bullet-}.2CO_2$, (C) $I_2^{\bullet-}.3CO_2$, (D) $I_2^{\bullet-}.4CO_2$, (E) $I_2^{\bullet-}.5CO_2$, (F) $I_2^{\bullet-}.6CO_2$, (G) $I_2^{\bullet-}.7CO_2$, (H) $I_2^{\bullet-}.8CO_2$, (I) $I_2^{\bullet-}.9CO_2$, and (J) $I_2^{\bullet-}.10CO_2$ clusters (I atom is treated by 6−311G(d) basis set). I atoms are shown by the largest violet spheres, the grey spheres correspond to C atoms, and the red spheres refer to O atoms of solvent CO_2 units in each structure of the solvated cluster. In each case, the distance between the two I atoms is ∼3.3−3.0 Å, the distance between C and I atoms is ∼3.9−4.9 Å.

parallel to I···I axis is also considered though. However, geometry optimization leads to the same structure as shown in Figure 1A. It is clearly observed from Figure 1A that the geometry of the solvent CO_2 unit in the cluster is slightly distorted from the isolated CO_2 structure in the presence of the $I_2^{\bullet-}$ system. Free CO_2 has a $D_{\infty h}$ point group with r_{CO}= 1.14 Å and ∠OCO = 180°. But in the cluster, CO_2 unit has a lower symmetry (C_{2v}) with a calculated bond distance and bond angle of 1.14 Å and 176.4°, respectively. Geometrical parameters of the cluster suggest that the solvent CO_2 molecule is bent by ∼3.6° in the solvated anion cluster system. This observation is in good agreement with the earlier reported theoretical data calculated at MP2/6−311G(d,p) level and larger than the experimental value by ∼1°.[28] CO bond length in this cluster remains unchanged compared to that of a free CO_2 unit.

The initial guess structures for the disolvated cluster are designed by the bottom-up approach. Out of four initial guesses, the relaxed, most stable structure of $I_2^{\bullet-}.2CO_2$ cluster is shown in Figure 1B where the second solvent CO_2 unit is attached from the opposite side of the first solvent CO_2 unit. Initial structures having both near perpendicular and parallel solvent CO_2 units with respect to the solute I···I axis are tried though. Both of the solvent CO_2 units are perpendicular to the I···I molecular axis in the most stable structure. In both the mono- and disolvated clusters, the distance between C and I atoms is calculated as ∼3.9 Å. The most favored structure of trisolvated cluster $I_2^{\bullet-}.3CO_2$ is shown in Figure 1C with calculated ∠OCO angle of 176.7−176.9°. Various initial guess structures for $I_2^{\bullet-}.4CO_2$ cluster are considered based on the minimum energy structure predicted for $I_2^{\bullet-}.3CO_2$ cluster, and the most stable structure is displayed in Figure 1D, where three CO_2 molecules are near perpendicular to the I···I axis. The calculated ∠OCO bond angles are ∼177°. Following the similar bottom-up approach, the initial guess structures for higher clusters of $I_2^{\bullet-}.nCO_2$ (n = 5−10) are considered followed by geometry optimization at BHHLYP/6−311+G(d) level of theory. The most stable structures for $I_2^{\bullet-}.nCO_2$ (n = 5−10) are displayed in Figure 1E−J. The calculated ∠OCO angles are varied from 176.8° to 177.3° in the most stable structure of $I_2^{\bullet-}.5CO_2$ cluster (structure shown in Figure 1E). Similar variation in calculated ∠OCO angles is observed for $I_2^{\bullet-}.nCO_2$ clusters (n = 6−10). It is observed that for clusters having more than five solvent CO_2 units, at least one solvent CO_2 unit is at a distance of more than 4.0 Å from solute $I_2^{\bullet-}$ unit. In contrast to the present observation, the previous theoretical prediction based on molecular dynamics simulation incorporating an empirical force field for solute−solvent as well as solvent−solvent interactions favors the successive addition of solvent CO_2 molecules in an asymmetric fashion.[18] This may be due to inaccurate treatment of solute−solvent and solvent−solvent interactions in these anionic clusters favoring induced dipole−induced dipole interaction between two solvent CO_2 molecules over ion-induced dipole interaction between the solute $I_2^{\bullet-}$ and solvent CO_2 molecules. To verify the influence of spin−orbit coupling in the equilibrium structure of these solvated clusters, geometry optimizations of the equilibrium structures are repeated including spin−orbit interaction at the same level of theory for n = 1 and 6 as test cases with no significant change in the optimized structures.

In summary, the calculated I···I bond distance is shorter than the isolated solute $I_2^{\bullet-}$ (3.334 Å) unit in all the solvated clusters, $I_2^{\bullet-}.nCO_2$ (n = 1−10). On each successive addition of solvent CO_2 units, the I···I distance decreases in all these solvated clusters. On the addition of ten solvent CO_2 molecules to the iodine dimer radical anion system $I_2^{\bullet-}$, a decrease of ∼0.3 Å in the I···I bond distance occurred. In all these cases, the structures obtained on full optimization applying the Newton−Raphson procedure are further optimized using the Monte−Carlo simulated annealing method to look for the global minimum energy structures. However, in all the cases the global structures predicted are very close to those obtained by applying the Newton−Raphson procedure. On refining these global minimum energy structures applying BHHLYP method, the same struc-

TABLE 2: Selected Geometrical, Valence, and Energy Parameters of the Most Stable Structure for Each Size (n) Cluster of $I_2^{\bullet-}.nCO_2$ ($n = 1-10$) at MP2/6-311+G(d) Level of Theory (I is treated by 6-311G(d) basis set)

species, $I_2^{\bullet-}.nCO_2$[a]	I···I bond distance (Å)[b]	charge transferred to CO_2 moiety (au)[b]	stabilization energy (E^{stab}), eV: theory (MP2)[c]	stabilization energy (E^{stab}), eV: expt[d]	ion−solvent interaction energy (E^{int-is}), eV[c]	solvent−solvent interaction energy (E^{int-ss}), eV[c]
$I_2^{\bullet-}.CO_2$ (2)	3.332	0.04	0.224, (0.232)	0.234	0.224, (0.232)	−
$I_2^{\bullet-}.2CO_2$ (4)	3.332	0.08	0.430, (0.442)	0.440	0.422, (0.435)	0.008, (0.008)
$I_2^{\bullet-}.3CO_2$ (4)	3.328	0.10	0.648	0.630	0.574	0.074
$I_2^{\bullet-}.4CO_2$ (4)	3.330	0.10	0.838	0.805	0.753	0.085
$I_2^{\bullet-}.5CO_2$ (4)	3.325	0.11	1.052	0.975	0.842	0.211
$I_2^{\bullet-}.6CO_2$ (4)	3.316	0.14	1.424	1.150	0.976	0.448
$I_2^{\bullet-}.7CO_2$ (5)	3.313	0.13	1.636	1.327	1.099	0.537
$I_2^{\bullet-}.8CO_2$ (5)	3.311	0.14	1.866	1.505	1.219	0.647
$I_2^{\bullet-}.9CO_2$ (5)	3.304	0.17	2.225		1.300	0.925
$I_2^{\bullet-}.10CO_2$ (5)	3.300	0.14	2.298		1.427	0.872

[a] Values in the parentheses show the number of minimum energy structures obtained. [b] Calculated at BHHLYP/6−311+G(d) level of theory. [c] Values in the parentheses are calculated at CCSD(T)/6−311+G(d) level (I is treated by 6−311G(d) set of basis function). [d] Reference 32

tures are obtained. This confirms that the predicted structures are truly global minimum energy structures. It is worth noting that in all these cases the calculated $\langle S_z^2 \rangle$ value is ∼0.75, suggesting no spin contamination of the wave functions for these doublet systems.

3.2. Valence Parameters. To see the effect of solvation on the distribution of the excess electron in the iodine dimer radical anion, $I_2^{\bullet-}$, Mulliken atomic spin ($\alpha-\beta$) population over different atoms is calculated in $I_2^{\bullet-}.nCO_2$ clusters ($n = 1-10$). It is observed that the odd electron spin is mainly populated over two I atoms in case of monosolvated cluster, $I_2^{\bullet-}.CO_2$, and it is equally distributed over two iodine atoms. It is also noticed that the spin distribution of the odd electron changes marginally on successive addition of solvent CO_2 molecules in $I_2^{\bullet-}.nCO_2$ clusters ($n = 2-10$). Mulliken and Lowdin population analysis also suggests that a major part of the excess charge is distributed mainly over the solute moiety in all the solvated clusters, $I_2^{\bullet-}.nCO_2$ ($n = 1-10$). The charge transfer observed from the solute iodine dimer radical moiety to solvent CO_2 units is ∼0.17 au in the case of $I_2^{\bullet-}.9CO_2$ cluster, and in the case of the monomer cluster it is ∼0.04 au. It is well-known that quantum chemical bond order index can provide important information on the type and extent of bonding between two atoms. Calculated bond order between two iodine atoms in free and solvated dimer radical anion $I_2^{\bullet-}.nCO_2$ ($n = 1-10$) suggests the presence of a sigma type hemi bond between two I atoms due to head-on overlapping of respective p-orbitals. It is also observed that such bonding remains insensitive to the successive addition of solvent CO_2 units.

3.3. Solvent Stabilization and Ion−Solvent Interaction Energy. The solvent stabilization energy of $I_2^{\bullet-}.nCO_2$ clusters can be expressed as

$$E^{stab} = E_{I_2^{-}.nCO_2} - (nE_{CO_2} + E_{I_2^{-}})$$

where $E_{I_2^-}.nCO_2$, E_{CO_2}, and $E_{I_2^-}$ refer to the total energy of the cluster $I_2^{\bullet-}.nCO_2$, the energy of a single solvent CO_2 molecule, and the energy of the bare $I_2^{\bullet-}$ system, respectively. Thus, E^{stab} essentially evaluates to the total interaction energy (ion−solvent interaction + solvent−solvent interaction) of the solute $I_2^{\bullet-}$ with n solvent CO_2 units around the solute in the solvated cluster of size n. The calculated solvent stabilization energy of the $I_2^{\bullet-}.nCO_2$ ($n = 1-10$) clusters are given in Table 2. The plot for the variation of E^{stab} vs n (cluster size) is displayed in Figure 2a to show that E^{stab} varies linearly with the number of solvent

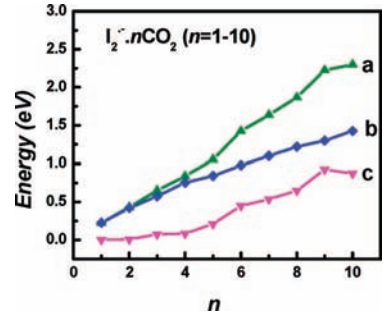

Figure 2. Variation of calculated (a) solvent stabilization energy (E^{stab}), (b) ion−solvent interaction energy (E^{int-is}), and (c) solvent−solvent interaction energy (E^{int-ss}) in eV with the number of solvent CO_2 molecules (n) in $I_2^{\bullet-}.nCO_2$ cluster ($n = 1-10$) at MP2/6−311+G(d) level of theory (I is treated by 6−311G(d) basis set).

CO_2 molecules in the solvated clusters and the variation of E^{stab} is best fitted by the following linear relation:

$$E^{stab} = -0.072 + 0.243.n$$

when E^{stab} is expressed in eV and n is the number of solvent CO_2 molecules. This linear fitted plot has correlation coefficient greater than 0.999. Stabilization energy for solvated cluster $I_2^{\bullet-}.nCO_2$ ($n = 1-10$) calculated by applying such a discrete model corresponds to the internal energy of the molecular clusters. The stabilization energy of the clusters (E^{stab}) increases with the increase in the number of solvent molecules accounting for ion−solvent interaction as well as solvent−solvent interaction. In other words, solvent stabilization energy does not saturate because it remains favorable to attach additional CO_2 molecules to the existing CO_2 network. The linear relationship between solvent stabilization energy (E^{stab}) and cluster size (n) suggests that on average the total interaction energy between the anionic solute $I_2^{\bullet-}$ and a solvent CO_2 molecule is ∼243 meV for small size clusters at MP2 level of theory. This average interaction energy is overestimated by ≤20% compared to the experimental determinations of Neumark and co-workers based on cluster calorimetric technique (see Table 2).[32]

The interaction between the solute iodine dimer radical anion $I_2^{\bullet-}$ and the solvent CO_2 cluster $(CO_2)_n$ known as interaction energy between ion and solvent ($E^{int\text{-}is}$) may be calculated by the following relation,

$$E = E_{I_2^{-}.nCO_2} - (E_{(CO_2)_n} + E_{I_2^{-}})$$

where $E_{I_2^{\bullet-}}.nCO_2$, $E_{(CO_2)_n}$ and $E_{I_2^{\bullet-}}$ refer to the energy of the cluster $I_2^{\bullet-}.nCO_2$, the energy of $(CO_2)_n$ system and the energy

of $I_2^{\bullet-}$ system respectively. The energy of the $(CO_2)_n$ system ($E_{(CO_2)n}$) is calculated by removing the solute part from the fully relaxed structure of the solvated cluster followed by single point energy calculation at the same level of theory. $E_{I_2^{\bullet-}}$ is also evaluated in the same way, i.e., by removing the solvent CO_2 units from the optimized structure of the cluster followed by single point energy calculation. The definition suggests that the interaction energy accounts for the net interaction of solute $I_2^{\bullet-}$ and the solvent CO_2 molecules eliminating intersolvent interactions. The calculated ion−solvent interaction energy for $I_2^{\bullet-}.nCO_2$ ($n = 1-10$) is tabulated in Table 2. The plot for the variation of $E^{\text{int-is}}$ vs n (cluster size) is depicted in Figure 2b. It is observed that $E^{\text{int-is}}$ also varies linearly with the number of solvent CO_2 molecules in the solvated clusters, and the variation of $E^{\text{int-is}}$ is best fitted by the following linear relationship:

$$E^{\text{int-is}} = 0.171 + 0.129.n,$$

when $E^{\text{int-is}}$ is expressed in eV and n is the number of solvent CO_2 molecules. This linear fitted plot has correlation coefficient >0.99. The linear relation suggests that the average interaction energy between the anionic solute and a solvent CO_2 molecule is ∼129 meV at MP2 level.

On subtracting the ion−solvent interaction ($E^{\text{int-is}}$) from the solvent stabilization energy (E^{stab}) of each cluster, the solvent−solvent interaction energy ($E^{\text{int-ss}}$) can be evaluated. The calculated solvent−solvent interaction energy ($E^{\text{int-ss}}$) of $I_2^{\bullet-}.nCO_2$ ($n = 1-10$) is tabulated in Table 2. The variation of $E^{\text{int-ss}}$ with size of the cluster (n) is also shown in Figure 2c. As the solvent CO_2 molecules are far apart, the calculated solvent−solvent interaction energy is close to zero for $I_2^{\bullet-}.nCO_2$ clusters ($n \leq 4$). For higher clusters, the solvent−solvent interaction energy increases asymptotically. In the present case, the solvent−solvent interaction energy has dispersion nature and originated from induced dipole−induced dipole interaction of solvent CO_2 molecules. It is worth mentioning that the calculated interaction energy between two solvent CO_2 molecules is ∼85 meV in the case of neutral $(CO_2)_n$ clusters ($n = 1-3$) at MP2/6−311+G(d) level of theory. The energy parameters for mono- and disolvated clusters are also calculated applying the CCSD(T) method, and the values are listed in Table 2. It is also worth mentioning that the basis set superposition error (BSSE) calculated for disolvated cluster $I_2^{\bullet-}.2CO_2$ following the counterpoise method is less than 5% and the BSSE for monosolvated cluster $I_2^{\bullet-}.CO_2$ is about 12%. The present calculated energy for solute−solvent (129 meV) and solvent−solvent (85 meV) interactions applying first-principle-based electronic structure theory justifies a rather symmetric successive addition of solvent CO_2 molecules to the ionic solute $I_2^{\bullet-}$ in contrast to the previous prediction of asymmetric successive addition applying classical MD simulation.

3.4. IR and Raman Spectra. As discussed in the earlier section, $I_2^{\bullet-}.nCO_2$ ($n = 1-10$) clusters are stabilized by the interaction between $I_2^{\bullet-}-CO_2$ (solute−solvent) as well as CO_2-CO_2 (solvent−solvent) interactions. Because of these interactions, it is expected that the normal modes of solute and solvent units in $I_2^{\bullet-}.nCO_2$ ($n = 1-10$) clusters get modified compared to that of free solute $I_2^{\bullet-}$ and solvent CO_2 units. Normal mode analysis for all the $I_2^{\bullet-}.nCO_2$ clusters ($n = 1-10$) and isolated $I_2^{\bullet-}$ and CO_2 systems has been carried out. IR and Raman spectra of these systems have been simulated. Lorentzian line shape has been applied with peak half-width of 10 cm^{-1} for all the vibrational spectral plots. Based on the literature data on the stretching and bending frequency modes of CO_2 ($\nu_{\text{bend}} = 667$ cm^{-1}, $\nu_{\text{sym}} = 1388$ cm^{-1}, and $\nu_{\text{asym}} = 2349$ cm^{-1}) and the present calculated values ($\nu_{\text{bend}} = 703$ cm^{-1}, $\nu_{\text{sym}} = 1466$ cm^{-1}, and $\nu_{\text{asym}} = 2547$ cm^{-1}) at BHHLYP/6−311+G(d) level of theory, the scaling factor is considered as 0.93 to account for the anharmonic nature of vibrations. The same scaling factor has been used for predicting the vibrational spectrum in all these clusters. Calculated scaled frequencies for free CO_2 are 653, 1363, and 2369 cm^{-1}, respectively, for bending (ν_{bend}), symmetrical stretching (ν_{sym}), and asymmetrical stretching (ν_{asym}), and the theoretical IR and Raman spectra are displayed in Figure 3 and Figure 4, respectively.

As the CO_2 molecule has a center of symmetry, the symmetric stretching mode is only Raman active, and other modes are IR active as shown in Figure 3i and Figure 4i. The only vibrational mode (91 cm^{-1}) of $I_2^{\bullet-}$ is also Raman active and shown in Figure 4ii. Calculated vibrational frequency for bending and asymmetric stretching mode of CO_2 of these solvated clusters $I_2^{\bullet-}.nCO_2$ ($n = 1-10$) are listed in Table 3. It is to be noted that symmetric stretching mode of CO_2 in these solvated clusters remains insensitive to the successive addition of solvent molecules. Scaled IR and Raman spectra for monosolvated cluster, $I_2^{\bullet-}.CO_2$ is shown in Figures 3ii and 4iii, respectively. The IR spectrum is characterized by a strong peak at 2332 cm^{-1} in asymmetric stretching region of C−O bond and a relatively weak band at ∼650 cm^{-1} in the bending region of C−O bond. The Raman spectra is characterized by a strong band at ∼90 cm^{-1} (corresponding to symmetric I−I stretch) and two weak bands at ∼650 cm^{-1} (corresponding to bending mode of CO_2) and 1346 cm^{-1} (corresponding to symmetric C−O stretching mode of CO_2). The interesting feature of this Raman spectrum is a band at ∼650 cm^{-1} (bending region of CO_2 molecule) and a very weak band at ∼2330 cm^{-1} (asymmetric C−O stretching region of CO_2), which are absent in the free CO_2 Raman spectrum (see Figure 4i). The $I_2^{\bullet-}.CO_2$ cluster is stabilized by $I_2^{\bullet-}$ and CO_2 interaction, and some amount of negative charge is also transferred to the solvent CO_2 moiety from the solute $I_2^{\bullet-}$ unit. As a result, the symmetry of the CO_2 molecule is distorted compared to the free solvent molecule and the symmetric bending mode becomes Raman active. The symmetric C−O stretching mode remains IR inactive as in the case of the free CO_2 system. Both the stretching modes of CO_2 are red-shifted compared to the free molecule ($-\Delta\nu_{\text{sym}} = 17$ cm^{-1} and $-\Delta\nu_{\text{asym}} = 37$ cm^{-1}), but the bending mode is both red- and blue-shifted compared to the free molecule ($\Delta\nu_{\text{bend}} = +5$ and -6 cm^{-1}) in this cluster. The degeneracy of the bending vibrational mode of CO_2 is lost in this anionic monosolvated cluster, $I_2^{\bullet-}.CO_2$. Two bands at 647 and 658 cm^{-1} are observed in the vibrational analysis and appeared as a small broad peak ∼650 cm^{-1} in both IR and Raman spectra compared to the free CO_2 molecule spectra. An extra band appeared at ∼650 cm^{-1} in the simulated Raman spectrum when the CO_2 molecule forms a molecular cluster with iodine dimer radical anion ($I_2^{\bullet-}$).

IR and Raman spectra of higher clusters ($n = 2-10$) are also simulated following the same procedure, and the two spectra for $I_2^{\bullet-}.10CO_2$ cluster are displayed in Figures 3iii and 4iv, respectively. The essential features of the IR spectra in all the higher clusters are similar to that of monosolvated cluster $I_2^{\bullet-}.CO_2$. However, differences are observed in the Raman spectra of these clusters on successive addition of solvent CO_2 molecules. The relative intensity of the Raman band corresponding to the symmetric stretching region of the C−O bond continuously increases on successive addition of solvent CO_2 units; the position of the band is insensitive to the number of solvent molecules though. The weak Raman band at ∼2330 cm^{-1} is most intense in the case of $I_2^{\bullet-}.9CO_2$ cluster. This may

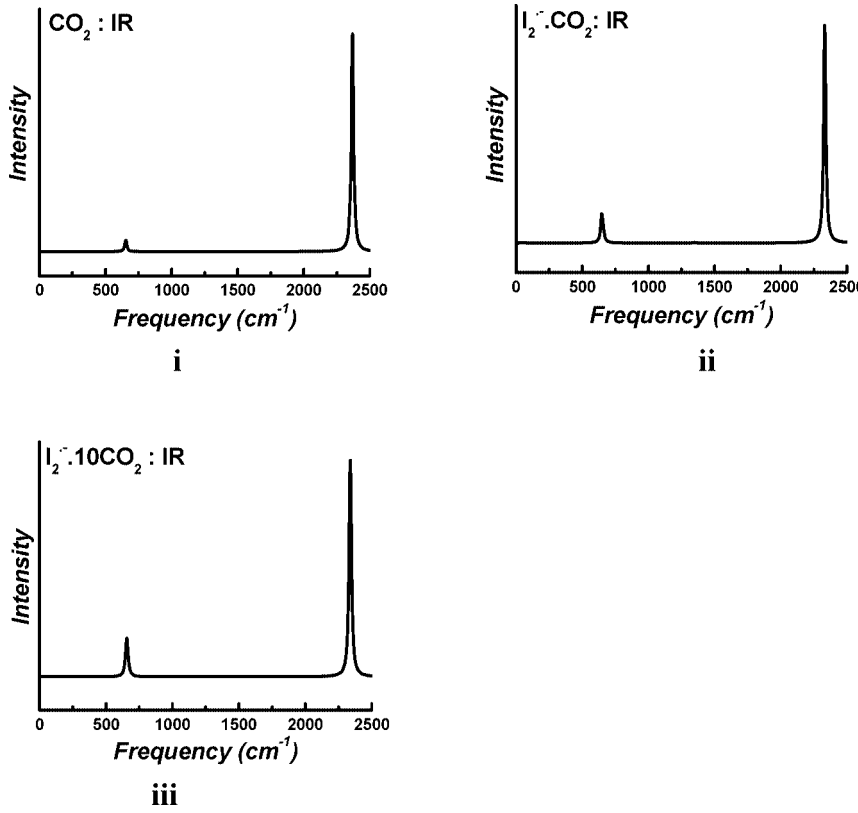

Figure 3. Scaled IR spectra of (i) isolated CO_2 molecule and solvated clusters (ii) $I_2^{\bullet-}.CO_2$ and (iii) $I_2^{\bullet-}.10CO_2$. A scaling factor of 0.93 is applied to account for the anharmonic nature of vibration. Lorentzian line shape has been applied with peak half-width of 10 cm^{-1} for all the IR plots.

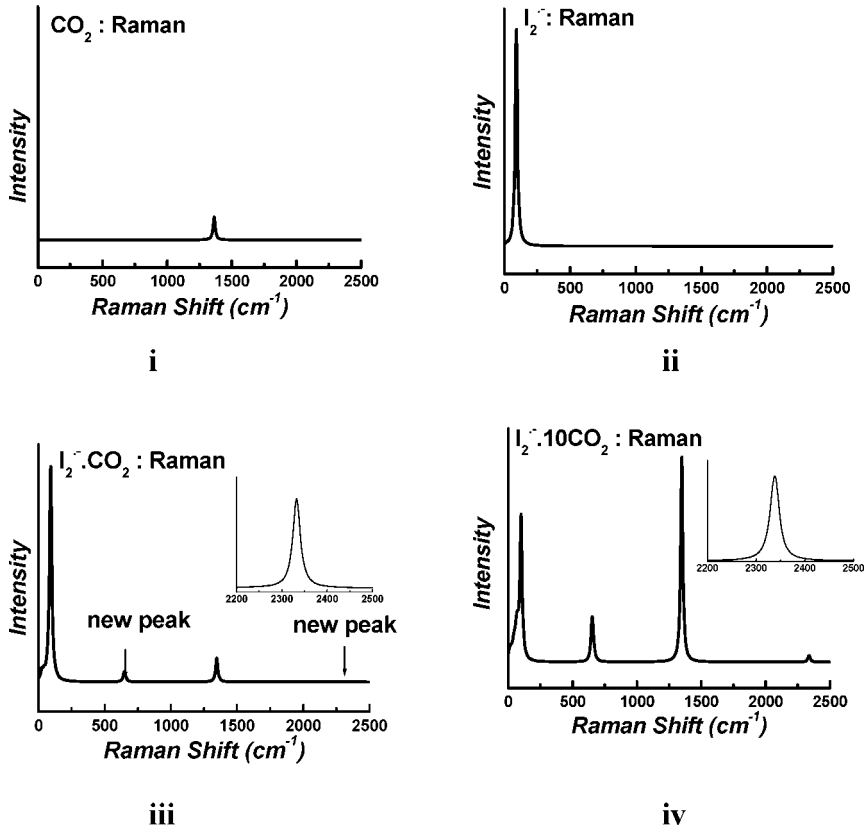

Figure 4. Scaled Raman spectra of an (i) isolated solvent CO_2 molecule and (ii) solute $I_2^{\bullet-}$ system. Raman spectra of solvated clusters (iii) $I_2^{\bullet-}.CO_2$ and (iv) $I_2^{\bullet-}.10.CO_2$. The same scaling factor of 0.93 is applied in the present cases. Lorentzian line shape has been applied with peak half-width of 10 cm^{-1} for all the spectral plots.

be due to the maximum charge transfer of the excess electrons to the solvent CO_2 units in this particular cluster (see Table 2).

In short, degeneracy of the bending mode of the free solvent CO_2 unit is lost when it interacts with the charged solute $I_2^{\bullet-}$

TABLE 3: Scaled Vibrational Frequency Calculated at BHHLYP/6-311++G(d,p) Level of Theory for Bending and Asymmetric Stretching Frequency of I_2 and CO_2 in $I_2^{\bullet-}.nCO_2$ ($n = 1-10$) Clusters (for I atom split valence 6-311G(d) basis set is adopted)[a]

species	I−I stretching, bending, and asymmetric stretching frequency of CO_2 (cm^{-1})[§]
$I_2^{\bullet-}.CO_2$	*92 (0, 140); 647(2,5), 658 (0.5, 1)*; 2332 (17, 0.2)
$I_2^{\bullet-}.2CO_2$	*92 (0, 132); 647 (4, 0.5), 651 (0.1, 6), 658 (0, 2), 659 (1, 0),*; 2332 (0.9, 0.1), 2333 (32.7, 0.1)
$I_2^{\bullet-}.3CO_2$	*92 (0, 127.6); 645 (1.3, 4.2), 648 (4.4, 1.7), 652 (0.7, 6.5), 658 (0.2, 1.9), 659 (1.4, 0.3), 660 (0.5, 0.5)*; 2332 (3.1, 0.1), 2334 (12, 0.5), 2335 (34, 0.4)
$I_2^{\bullet-}.4CO_2$	*93 (0, 101); 646 (1.5, 3), 648 (2.9, 2.5), 649 (2.8, 4.5), 654 (1, 3.7), 659 (0, 0.9), 659 (0.3, 1.3), 660 (1.9, 0.5), 661 (0.3, 0.4)*; 2326 (0.6, 0.1), 2332 (13.8, 0.4), 2337 (36.2, 0.1), 2339 (13.6, 0.4)
$I_2^{\bullet-}.5CO_2$	*93 (0, 100); 646 (1, 2.9), 647 (1.5, 3.8), 649 (4.3, 3.2), 653 (0.6, 3.0), 656 (0, 0.9), 656 (0.7, 0.7), 659 (2, 0.7), 660 (1.6, 0.6), 661 (0.9, 0.3), 661 (1.4, 0.7)*; 2327 (1.2, 0.1), 2332 (11, 0.3), 2336 (14.6, 0), 2338 (39.1, 0.1), 2340 (15.2, 0.1)
$I_2^{\bullet-}.6CO_2$	*93 (0, 83);647 (0.4, 7.2), 648 (0.8, 3.2), 649 (0.7, 4.3), 651 (1.7, 1), 654 (0.3, 2.5), 656 (0.1, 0.1), 657 (2.9, 0.3), 657 (5.7, 0.2), 658 (1.7, 0.7), 659 (1.4, 2.1), 660 (0.8, 1.6), 663 (1.5, 2.9)*; 2330 (1.1, 0.1), 2331 (4.7, 0.2), 2333 (15.5, 0.2), 2335 (51, 0.5), 2337 (20.5, 0.6), 2339 (5.5, 0.6)
$I_2^{\bullet-}.7CO_2$	*95 (0, 98.5);647 (0.7, 3.8), 648 (0.2, 5.8), 649 (1.8, 3.1), 650 (2.1, 3.7), 651 (0.4, 2), 655 (1.3, 0.2), 656 (2.5, 0.4), 656 (3.4, 1), 657 (2, 1.2), 658 (0.8, 0.6), 658 (0.6, 1), 658 (1.9, 0.4), 660 (0.4, 0.8), 663 (2.7, 2.3)*; 2329 (2.5, 0.2), 2332 (3. 0.2), 2335 (27.6, 0.2), 2336 (38.6, 0.3), 2338 (6.9, 1.7), 2338 (30.1, 0.3), 2342 (5.7, 0.2)
$I_2^{\bullet-}.8CO_2$	*95 (0, 103.4); 648 (1.3, 2.6), 648 (0.4, 3.3), 648 (0.6, 4.3), 649 (1.1, 5.1), 650 (1.3, 0.4), 651 (1, 5.6), 654 (0, 0.6), 655 (5.7, 0.6), 656 (2.4, 0.2), 657 (1.2, 0.9), 657 (0.1, 0.4), 658 (1.5, 1), 659 (1.7, 0.2), 660 (0.9, 0.5), 661 (0.6, 0.9), 664 (3.7,1.7)*; 2326 (8.7, 0.1), 2332 (4.8, 0.1), 2334 (24.9, 0.8), 2335 (26.2, 0.1), 2338 (26.7, 0.8), 2339 (17.7, 0.6), 2341 (18.2, 0.2), 2343 (5, 0.3)
$I_2^{\bullet-}.9CO_2$	*97 (0, 88);646 (0.4, 3.7), 650 (1, 2.7), 650 (0.5, 4.2), 651 (0.2, 4), 652 (0.4, 1), 652 (0.1,2.1), 653 (1.7, 1.2), 653 (0.2, 0.8), 655 (3.2, 1.2), 656 (0, 0.8), 656 (0.5, 1.2), 657 (1.3, 0.4), 658 (0.8, 1.3), 659 (3.9,4.5), 659 (1.7,0.8), 660 (2.5, 0.3), 660 (5.6, 1), 667 (4.8, 1.7)*; 2329 (7.9, 0.1), 2331 (26.6, 1.5), 2333 (8, 0.6), 2336 (3.3, 1.4), 2337 (24.2, 0.7), 2338 (25.9, 1.4), 2340 (35.3, 0.3), 2342 (9.8, 0.8), 2343 (7.4, 0.7)
$I_2^{\bullet-}.10CO_2$	*98 (0,102), 648 (0, 3.4), 648 (1, 2.1), 650 (1.2, 8.4), 650 (0.9, 2.5), 651 (0.7, 1.9), 652 (3.7, 1.8), 653 (0.1, 2.4), 654 (1.4, 4.3), 655 (0.5, 1.3), 655 (1, 0.5), 656 (3.2, 2), 656 (3.6, 0.7), 656 (0.7, 1.3), 657 (0.3, 0.2), 658 (1.1, 1.2), 659 (1.7, 1.2), 659 (2.7, 0.4), 660 (2.3, 0.1), 660 (1.9, 2), 666 (3, 2)*; 2328 (8.2, 0.3), 2333 (2.8, 0.1), 2334 (1.8, 0.2), 2334 (8.9, 0.5), 2337 (32.8, 0.5), 2338 (46.6, 1), 2339 (16.3, 1.2), 2340 (6.5, 0.7), 2341 (31.9, 0.7), 2343 (7.2, 0.6)

[a] A scaling factor of 0.93 is applied to account for the anharmonic nature of vibration. [b] Values in the parentheses refer to intensities of IR (in $debye^2\ amu^{-1}angstrom^{-2}$) and Raman (in $angstrom^4\ amu^{-1}$) modes.

to form a molecular cluster. Two vibrational bands are observed at the bending region (~650 cm^{-1}) of CO_2 in normal-mode analysis. Both the stretching modes of CO_2 are red-shifted compared to the free molecule, but the bending mode is both red- and blue-shifted compared to the free molecule in these solvated clusters. Plots showing IR spectra of $I_2^{\bullet-}$ nCO_2 ($n = 1-10$) clusters show similar features. The vibrational band at the bending region of CO_2 (~650 cm^{-1}) in the Raman spectra is a characteristic feature for the formation of $I_2^{\bullet-}.CO_2$ cluster. A weak band in the asymmetric stretching region (~2330 cm^{-1}) of the CO_2 vibration appears in the Raman spectra in these solvated clusters, and the band is the most intense for $I_2^{\bullet-}.9CO_2$ cluster.

4. Conclusions

Structure, energy, and IR and Raman spectra of $I_2^{\bullet-}.nCO_2$ clusters ($n = 1-10$) are reported in this study of the process of microsolvation of the negatively charged solute $I_2^{\bullet-}$ in carbon dioxide. Hybrid density functional (BHHLYP) is applied to study the structural aspects of the present solvated clusters with a split valence 6−311+G(d) basis function. Monte−Carlo-based simulated annealing procedure is also applied to determine the global minimum energy structure. It is observed that symmetric successive addition of solvent CO_2 molecules is favored to the anionic solute in these clusters. Solvent stabilization and interaction energies are calculated applying MP2 as well as CCSD(T) theory. It is observed that both the solvent stabilization as well as interaction energy continuously increases with the successive addition of solvent CO_2 units. Calculated solute−solvent interaction energy is higher that solvent−solvent interaction energy by ~44 meV in these ionic clusters. Simulated IR spectra of all the solvated $I_2^{\bullet-}$ nCO_2 clusters ($n = 1-10$) show similar features. When the solvent CO_2 unit interacts with the charged solute $I_2^{\bullet-}$ to form a molecular cluster, the linearity of the CO_2 unit is lost, and as a result, degeneracy of the bending mode of free solvent CO_2 unit is lifted. The vibrational band at the

bending region of CO_2 in the Raman spectra is a characteristic feature for the formation of $I_2^{\bullet-}.CO_2$ cluster.

Acknowledgment. Sincere thanks are due to Computer Centre, BARC, for providing the ANUPAM parallel computing facility. A.K.P. and D.K.M. thank Dr. S. K. Sarkar and Dr. S. K. Ghosh for their constant support and encouragement.

References and Notes

(1) Ohtaki, H.; Radani, T. *Chem. Rev.* **1993**, *93*, 1157.
(2) Robertson, W. H.; Diken, E. G.; Price, E. A.; Shin, J. W.; Johnson, M. A. *Science* **2003**, *299*, 1367.
(3) Weber, J. M.; Kelley, J. A.; Nielson, S. B.; Ayotte, P.; Johnson, M. A. *Science* **2000**, *287*, 2461.
(4) Ayotte, P. G.; Weddle, H.; Kim, J.; Johnson, M. A. *J. Am. Chem. Soc.* **1998**, *120*, 12361.
(5) Ayala, R.; Martinez, J. M.; Pappalardo, R. R.; Marcos, E. S. *J. Chem. Phys.* **2003**, *119*, 9538.
(6) Masamura, M. *J. Chem. Phys.* **2003**, *118*, 6336.
(7) Bryce, R. A.; Vincent, M. A.; Malcolm, N. O. J.; Hillier, I. H. *J. Chem. Phys.* **1998**, *109*, 3077.
(8) Vaughn, S. J.; Akhmatskaya, E. V.; Vincent, M. A.; Masters, A. J.; Hillier, I. H. *J. Chem. Phys.* **1999**, *110*, 4338.
(9) Xantheas, S. S. *J. Am. Chem. Soc.* **1995**, *117*, 10373.
(10) Lehr, L.; Zannai, M. T.; Frischkorn, C.; Weinkauf, R.; Neumark, D. M. *Science* **1999**, *284*, 635.
(11) Chen, H-.Y.; Shew, W.-S. *J. Am. Chem. Soc.* **2000**, *122*, 7534.
(12) Dang, L. X.; Garret, B. C. *J. Chem. Phys.* **1993**, *99*, 2972.
(13) Markovich, G.; Pollac, S.; Giniger, R.; Cheshnovosky, O. *J. Chem. Phys.* **1994**, *101*, 9344.
(14) Majumdar, D.; Kim, J.; Kim, K. S. *J. Chem. Phys.* **2000**, *112*, 101.
(15) Pathak, A. K.; Mukherjee, T.; Maity, D. K. *J. Chem. Phys.* **2006**, *124*, 024322. Pathak, A. K.; Mukherjee, T.; Maity, D. K. *J. Chem. Phys.* **2006**, *125*, 074309. Pathak, A. K.; Mukherjee, T.; Maity, D. K. *J. Chem. Phys.* **2007**, *127*, 044304.
(16) Pathak, A. K.; Mukherjee, T.; Maity, D. K. *J. Phys. Chem. A* **2008**, *112*, 3399.
(17) Parson, R.; Faeder, J.; Delaney, N. *J. Phys. Chem. A* **2000**, *104*, 9653.
(18) Sanov, A.; Lineberger, W. C. *Phys. Chem. Commun.* **2002**, *5*, 165.
(19) Greenblatt, B. J.; Zanni, M. T.; Neumark, D. M. *Science* **1997**, *276*, 1675.
(20) Nandi, S.; Sanov, A.; Delaney, N.; Faeder, J.; Parson, R.; Lineberger, W. C. *J. Phys. Chem. A* **1998**, *102*, 8827.
(21) Asmis, K. R.; Taylor, T. R.; Xu, C.; Neumark, D. M. *J. Chem. Phys.* **1998**, *109*, 4389.
(22) Ladanyia, B. M.; Parson, R. *J. Chem. Phys.* **1997**, *107*, 9326.
(23) Sanov, A.; Sanford, T.; Nandi, S.; Lineberger, W. C. *J. Chem. Phys.* **1999**, *111*, 664.
(24) Papanikolas, J. M.; Maslen, P. E.; Parson, R. *J. Chem. Phys.* **1995**, *102*, 2452.
(25) Papanikolas, J. M.; Vorsa, V.; Nedal, M. E.; Campagnola, P. J.; Gord, J. R.; Lineberger, W. C. *J. Chem. Phys.* **1992**, *97*, 7002.
(26) Papanikolas, J. M.; Vorsa, V.; Nedal, M. E.; Campagnola, P. J.; Buchenau, H. K; Lineberger, W. C. *J. Chem. Phys.* **1993**, *99*, 8733.
(27) Davis, A. V.; Wester, R.; Bragg, A. E.; Neumark, D. M. *J. Chem. Phys.* **2003**, *119*, 2020.
(28) Gomez, H.; Taylor, T. R.; Neumark, D. M. *J. Chem. Phys.* **2002**, *116*, 6111.
(29) Margulis, C. J.; Coker, D. F. *J. Chem. Phys.* **1999**, *110*, 5677.
(30) Delaney, N.; Faeder, J.; Maslen, P. E.; Parson, R. *J. Phys. Chem. A* **1997**, *101*, 8147.
(31) Pathak, A. K.; Mukherjee, T.; Maity, D. K. *J. Chem. Phys.* **2007**, *126*, 034301.
(32) Wester, R.; Davis, A. V.; Bragg, A. E.; Neumark, D. M. *Phys. Rev. A* **2002**, *65*, 051201.
(33) Gopalakrishnan, S.; Liu, D.; Allen, H. C.; Kuo, M.; Shultz, M. J. *Chem. Rev.* **2006**, *106*, 1155.
(34) Wu, D.; Duan, S.; Liu, X.; Xu, Y.; Jiang, Y.; Ren, B.; Xu, X.; Lin, S. H.; Tian, Z. *J. Phys. Chem. A* **2008**, *112*, 1313.
(35) Braïda, B.; Hiberty, P. C.; Savin, A. *J. Phys. Chem. A* **1998**, *102*, 7872.
(36) Maity, D. K. *J. Phys. Chem. A* **2002**, *106*, 5716.
(37) Day, P. N.; Pachter, R.; Gordon, M. S.; Merrill, G. N. *J. Chem. Phys.* **2000**, *112*, 2063.
(38) Schmidt, M. W.; Baldridge, K. K.; Boatz, J. A.; Elbert, S. T.; Gordon, M. S.; Jensen, J. H.; Koseki, S.; Matsunaga, N.; Nguyen, K. A.; Su, S. J.; Windus, T. L.; Dupuis, M.; Montgomery, J. A. *J. Comput. Chem.* **1993**, *14*, 1347.
(39) Schaftenaar, G.; Noordik, J. H. *J. Comput.-Aided Mol. Des.* **2000**, *14*, 123.

JP805348Q